Dendrimer Probes for Enhanced Photostability and Localization in Fluorescence Imaging

Younghoon Kim,[†] Sung Hoon Kim,[‡] Melikhan Tanyeri,[†] John A. Katzenellenbogen,[‡] and Charles M. Schroeder[†‡§¶*]

[†]Department of Chemical and Biomolecular Engineering, [‡]Department of Chemistry, [§]Department of Materials Science and Engineering, and [¶]Center for Biophysics and Computational Biology, University of Illinois at Urbana-Champaign, Urbana, Illinois

ABSTRACT Recent advances in fluorescence microscopy have enabled high-resolution imaging and tracking of single proteins and biomolecules in cells. To achieve high spatial resolutions in the nanometer range, bright and photostable fluorescent probes are critically required. From this view, there is a strong need for development of advanced fluorescent probes with molecular-scale dimensions for fluorescence imaging. Polymer-based dendrimer nanoconjugates hold strong potential to serve as versatile fluorescent probes due to an intrinsic capacity for tailored spectral properties such as brightness and emission wavelength. In this work, we report a new, to our knowledge, class of molecular probes based on dye-conjugated dendrimers for fluorescence imaging and single-molecule fluorescence microscopy. We engineered fluorescent dendritic nanoprobes (FDNs) to contain multiple organic dyes and reactive groups for target-specific biomolecule labeling. The photophysical properties of dye-conjugated FDNs (Cy5-FDNs and Cy3-FDNs) were characterized using single-molecule fluorescence microscopy, which revealed greatly enhanced photostability, increased probe brightness, and improved localization precision in high-resolution fluorescence imaging compared to single organic dyes. As proof-of-principle demonstration, Cy5-FDNs were used to assay single-molecule nucleic acid hybridization and for immunofluorescence imaging of microtubules in cytoskeletal networks. In addition, Cy5-FDNs were used as reporter probes in a single-molecule protein pull-down assay to characterize antibody binding and target protein capture. In all cases, the photophysical properties of FDNs resulted in enhanced fluorescence imaging via improved brightness and/or photostability.

INTRODUCTION

Recent advances in fluorescence imaging and single-molecule fluorescence microscopy (SMFM) have enabled the direct observation of biological processes at the molecular level (1–6). Fluorescence imaging techniques critically rely on bright and photostable fluorescent probes with robust photophysical properties. Despite recent progress, there is a strong need for development of advanced fluorescent probes with small sizes and robust photophysical properties for biological imaging. Currently available fluorescent probes for biological labeling include genetically encoded fluorescent proteins (2,7), organic dyes (1,8), and semiconductor nanocrystals or quantum dots (QDs) (9,10). Organic dyes are typically brighter than genetically encoded fluorescent proteins due to enhanced quantum yields and/or molar absorption coefficients. Moreover, the photophysical properties of many organic dyes can be enhanced using reducing agents and oxygen scavenger systems (11–13). Single organic dye molecules are also small in size (<1 nm), which facilitates nonperturbative biomolecule labeling. However, organic dyes and fluorescent proteins generally suffer from rapid irreversible photobleaching, which can limit the study of some biological processes. Inorganic nanoconjugates such as QDs are exceptionally bright and have photostable fluorescent probes with narrow emission spectra over a wide range of wavelengths (14,15). However, compared to single organic dyes, biocompatible QDs are relatively large in size (~10–20 nm) due to their core/shell structure (16,17).

In this work, we report a new, to our knowledge, class of fluorescent probes based on chemically modified, multidye-labeled dendritic polymers. Biocompatible probes with small dimensions (<10 nm) are critically required for biological imaging and high-resolution fluorescence microscopy (18). To address this issue, we synthesized fluorescent dendritic nanoprobes (FDNs) to contain multiple covalently linked organic dyes on nanometer-sized macromolecules, thereby generating bright and photostable probes for fluorescence imaging. Dye-conjugated dendrimers are compact in size (~5 nm) and show superior spectral properties compared to single organic dyes. Dendrimers are polymers having highly regular branched structures with large numbers of terminal functional groups (19,20). Compared to linear macromolecules, dendrimers can be synthesized with controlled shapes and nearly monodisperse sizes, which is a key advantage for fluorescent probes used for biological labeling. Over the past several years, dendrimers have been used for gene and drug delivery (21) and diagnostic applications via live cell or animal imaging (22). Fluorescent dendrimers have been studied previously, but for different purposes, including synthetic light-harvesting macromolecules (23,24), aromatic

Submitted September 22, 2012, and accepted for publication January 28, 2013.

*Correspondence: cms@illinois.edu

Editor: Ashok Deniz.

0006-3495/13/04/1566/10 $2.00

http://dx.doi.org/10.1016/j.bpj.2013.01.052

nonaqueous dendrimers (25–28), polyphenylene dendrimers for bioassays (29,30), and optically active dendrimers that complex DNA (31–34). Our work aims to capitalize on the advantageous photophysical properties of multidye dendritic nanoconjugates to develop a new class, to our knowledge, of versatile and functional molecular probes for fluorescence imaging and sensing.

Dendritic nanoconjugates have an intrinsic capacity for broad chemical and functional versatility. From this perspective, dendrimers can be viewed as well-defined molecular scaffolds for assembling multiple fluorescent dyes and chemical functional groups onto single nanoscale probes. In this work, we use polyamidoamine (PAMAM) dendrimers, which serve as an ideal chemical platform for building synthetic nanoprobes. PAMAM dendrimers exhibit high degrees of water solubility and allow for facile surface functionalization via terminal amine groups, thereby enabling conjugation of multiple organic dyes via *N*-hydroxysuccinimide (NHS) ester linkages (35,36). In particular, we synthesized FDNs conjugated with multiple cyanine dyes, including both Cy5-FDNs and Cy3-FDNs. We further modified dendrimer scaffolds with various chemical functional groups, including biotin and dibenzocyclooctyne (DBCO) for copper-free click chemistry, which facilitates target-specific conjugation to biomolecules (37).

Using SMFM, we show that single dendritic nanoprobes bearing multiple cyanine dyes exhibit enhanced photophysical properties compared to single dye molecules, including exceptional photostability and increased brightness. In particular, single-molecule studies of FDNs reveal substantially increased fluorescence photobleaching lifetimes, defined as fluorescence on-time before bleaching to an effectively permanent dark state. Molecular probes with increased photobleaching lifetimes are critical for enabling long timescale observation of biological events using fluorescence imaging. By contrast, many organic dyes exhibit relatively short photobleaching lifetimes, especially for dyes with fluorescence emission wavelengths in the red region of the spectrum (600–700 nm), which can significantly limit the observation time for bulk-level and single-molecule fluorescence imaging studies (8).

Beyond nanoprobe synthesis and photophysical characterization, we directly applied FDNs to nucleic acid and protein assays using SMFM. We show that FDNs can be localized with nanometer-scale precision, superior to the localization precision achieved from the constituent single dyes when studied in isolation, which is a direct consequence of increased fluorescence emission intensities resulting from the multichromophoric nanostructures. In addition, we directly used Cy5-FDNs to assay single-molecule nucleic acid hybridization and for immunofluorescence imaging of microtubules in cytoskeletal networks. We further demonstrate proof-of-principle application of Cy5-FDNs to study protein-protein interactions at the single-molecule level using a single-molecule protein pull-down (SiMPull) assay (38). In all cases, FDNs exhibit robust photophysical properties and appear to hold strong potential as a new class of bright and photostable molecular probes for biological labeling and imaging.

MATERIALS AND METHODS

Chemical synthesis of dendritic nanoprobes

Multiple amine-reactive Cy5-NHS or Cy3-NHS ester dyes were linked to generation-5 (G5) or generation-6 (G6) PAMAM-amine dendrimers (Scheme S1 in the Supporting Material). G5 and G6 PAMAM dendrimers are ~5 and ~6 nm in diameter and nominally contain 128 and 256 surface amine groups, respectively. PAMAM dendrimers were further functionalized with biotin for affinity labeling or DBCO for click chemistry to enable target-specific labeling of biomolecules or surface immobilization for SMFM. After each successive addition reaction, the average degree of dye or chemical substitution was quantified by MALDI-TOF (matrix-assisted laser desorption/ionization time of flight) mass spectrometry analysis (see the Supporting Material). In this way, we could control the extent of fluorescent dye loading between ~1 and 15 dye molecules for PAMAM dendrimers. To prevent additional reactions or premature degradation, a fraction of the amine groups on PAMAM dendrimer surfaces was blocked with acetyl groups. At neutral pH, the remaining amine groups are protonated to yield surface ammonium ions ($R\text{-}NH_3^+$). Following chemical synthesis and purification, FDNs remained stable for several months upon storage at 4°C.

Photophysical characterization of dendritic nanoprobes

The photophysical properties of FDNs were characterized using bulk fluorescence spectrophotometry and SMFM. Bulk fluorescence emission and absorption spectra of FDN samples were obtained using a fluorescence spectrophotometer (Varian Eclipse). Single-molecule images of FDNs were obtained using an inverted microscope (Olympus IX-71) equipped for total internal reflection fluorescence microscopy (TIRF-M). Images were acquired using an electron multiplying charge-coupled device (EMCCD) camera (Andor iXonEM+). For SMFM experiments, fluorescent probes were immobilized on glass coverslip surfaces using copper-free click chemistry. First, glass coverslips were functionalized with PEG/PEG-biotin, followed by successive incubation with NeutrAvidin and a biotin-azide linker (Pierce). Next, DBCO-modified FDNs or DBCO-Cy5 dyes were covalently linked to glass coverslips through Cu-free click reaction with surface azide groups. Where indicated, FDNs and single Cy5 or Cy3 molecules were imaged in the presence of an oxygen scavenger system (glucose oxidase/catalase, Sigma) to minimize photobleaching. For comparative purposes, we also imaged FDNs and single Cy5 or Cy3 molecules in the absence of the oxygen scavenger system. Beyond proof-of-principle photophysical characterization experiments, Cy5-FDNs were used for DNA hybridization and an antibody binding assay by SiMPull. (see the Supporting Material).

RESULTS AND DISCUSSION

FDNs were synthesized by conjugating multiple organic dyes to generation-5 (G5) and generation-6 (G6) PAMAM dendrimers (Fig. 1). In this way, dendrimer molecules serve as molecular scaffolds to assemble multiple organic dyes and functional groups (Fig. 1 *a*), thereby generating fluorescent probes with nanoscale dimensions. A schematic of an FDN probe for illustrative purposes is shown in Fig. 1 *a*,

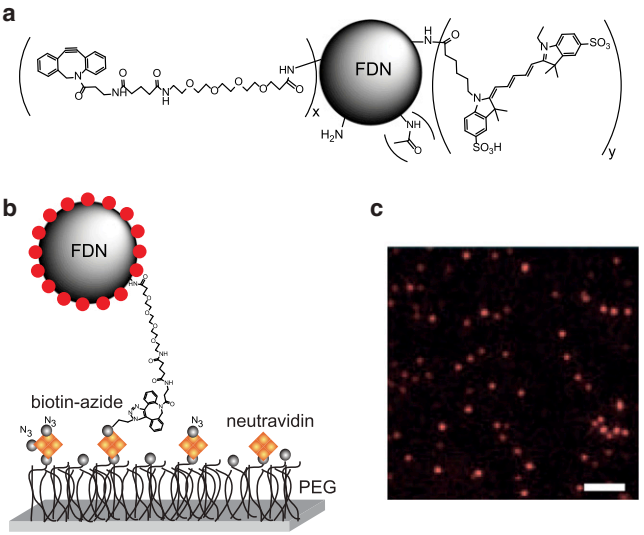

FIGURE 1 Dendrimer-based probes for fluorescence microscopy. (*a*) Schematic of FDNs, wherein multiple Cy5 dye molecules are conjugated to single PAMAM dendrimer molecules. Dendrimer surfaces are functionalized with DBCO to enable target-specific biochemical labeling using copper-free click chemistry. (*b*) Surface chemistry for single-molecule studies of FDNs, which are specifically linked to coverslip surfaces using copper-free click chemistry. (*c*) Single-molecule image of Cy5-FDNs. Scale bar: 3 μm.

and the full chemical structure of a PAMAM dendrimer conjugated with Cy5 dyes is shown in Scheme S1. Tables S1–S4 contain a summary of custom-modified dendritic nanoprobes used in this work (see the Supporting Material). In all cases, the average degree of chemical substitution on the FDNs can be accurately controlled through the reagent-to-dendrimer stoichiometry. Through a sequence of chemical conjugation reactions, we prepared Cy5-FDNs in which the number of chemical groups attached to the FDN surface could be controlled with narrow average values, as determined by MALDI-TOF mass spectrometry analysis. In this way, the average values of the number of Cy5 (or Cy3), biotin, DBCO, and acetyl groups attached to the FDN surface could be adjusted over the broad ranges of 1–15, 0–10, 0–10, and 0–80, respectively. Although the average range of chemical substitution can be tightly controlled, chemical conjugation will yield a distribution of occupancy within the dendrimer sample. Nevertheless, mass spectrometry analysis showed a low sample polydispersity index (PDI = 1.02) that remained constant before and after chemical coupling reactions (Tables S1–S4). Therefore, we concluded that no agglomeration occurred in the dendrimer samples before or after chemical conjugation, and the dendrimer molecules were fairly monodisperse. We further used PEGylation and/or acetylation to cap some of the remaining terminal primary amine groups on dendrimer surfaces, which minimizes nonspecific interactions with biomolecules and facilitates target-specific protein labeling. Surface capping of terminal amine groups by acetylation prevented premature degradation of PAMAM dendrimers by inhibiting subsequent and undesired side reactions.

Following synthesis and chemical analysis of Cy5-FDNs, we characterized the photophysical properties of these probes using SMFM. First, single Cy5-FDNs were immobilized on glass coverslip surfaces using specific chemical linkages (Fig. 1 *b*). PEGylated glass coverslips containing a mixture of PEG/PEG-biotin were treated with NeutrAvidin, rinsed thoroughly, and incubated with a biotin-azide linker. Next, DBCO-modified Cy5-FDNs or organic dyes were incubated with the azide-modified coverslips, thereby immobilizing fluorescent probes directly to surfaces using copper-free click chemistry (37). Overall, this approach yields single isolated Cy5-FDNs specifically linked to coverslip surfaces through biotin-avidin interactions, which is a common strategy for biomolecule immobilization (1,8). Single-molecule images of Cy5-FDNs are shown in Fig. 1 *c*.

We determined the localization precision and fluorescence emission intensities for single Cy5-FDNs and single Cy5 dyes (Fig. 2). Importantly, Cy5-FDNs are substantially brighter probes compared to single organic dyes (Fig. 2, *c* and *f*). The average fluorescence emission intensity for Cy5-FDNs bearing ~8 Cy5 dyes is ~4 times larger than a single Cy5 dye under the same excitation conditions, which results in a substantially improved signal/noise ratio for Cy5-FDNs (Fig. S1). For the imaging conditions used here, the fluorescence signal given by the EMCCD camera is directly proportional to the number of detected photons, which suggests that a larger number of photons is collected from Cy5-FDNs. Pixelated digital images show that both single Cy5-FDNs (Fig. 2 *c*, *inset*) and single Cy5 molecules (Fig. 2 *f*, *inset*) appear as diffraction-limited spots, which is expected based on Abbe's criterion for diffraction-limited optics, where the minimum resolvable feature size is $R = \lambda/2NA \approx 230$ nm for a wavelength $\lambda \approx 665$ nm and numerical aperture $NA = 1.4$.

Although single nanoprobes appear as diffraction-limited spots, the spatial position of any probe can be determined with arbitrarily small (nanometer or subnanometer) precision, provided that enough photons are collected. Several techniques have been developed for subdiffraction limit imaging of biological samples. Fluorescence imaging with one nanometer accuracy has been used to monitor intracellular events with nanometer-scale spatial resolution (1–10 nm), including real-time tracking of motor proteins (39–41). Recent advances in super-resolution microscopy have enabled the direct observation of cellular events beyond the diffraction limit (2,5), including stimulated emission depletion microscopy (42,43), wide-field structured illumination (44), and single-molecule techniques based on photoswitchable fluorescent probes including stochastic optical reconstruction microscopy (45,46), ground-state depletion microscopy followed by individual molecule return (47), and photoactivated localization

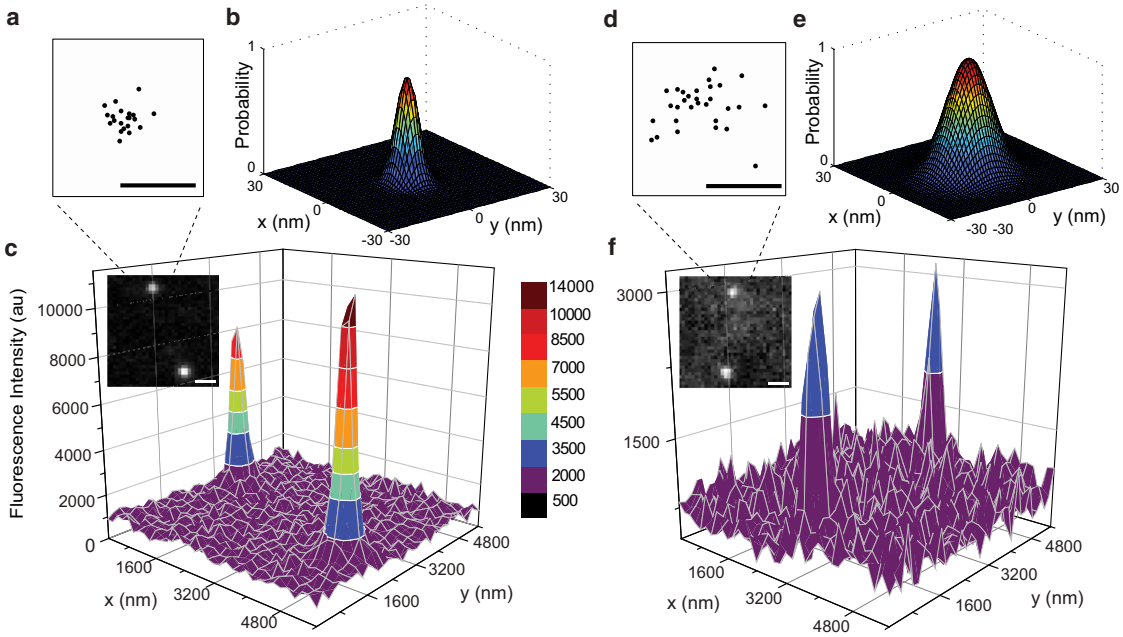

FIGURE 2 Localization precision and fluorescence intensity plots for single molecules of (*a–c*) Cy5-FDNs and (*d–f*) Cy5 dyes. (*a* and *d*) Distribution of centroid positions for a single Cy5-FDN and a single Cy5 dye, respectively (scale bar: 20 nm). Centroid positions for fluorescent probes were determined by Gaussian mask estimation over successive images. (*b* and *e*) two-dimensional Gaussian fits to the distributions of centroid position were used to determine localization precisions of 14 nm for Cy5-FDNs and 23 nm for single Cy5 dyes, expressed as the FWHM of the two-dimensional Gaussian fit. (*c* and *f*) Diffraction-limited fluorescence intensity plots for single Cy5-FDN molecules and single Cy5 dye molecules, respectively, showing that Cy5-FDNs are significantly brighter compared to single Cy5 dye molecules (scale bar: 1 μm). In all cases, Cy5-FDNs and single Cy5 dyes were imaged using the same excitation conditions.

microscopy (2,48). Spatial resolutions in the range of ~20 and 30 nm are typically achieved using single organic dyes or fluorescent proteins in stochastic optical reconstruction microscopy and photoactivated localization microscopy (3,5,45,49).

We determined the localization precision for single Cy5-FDNs using single-molecule imaging (Fig. 2 and Fig. S2). In these experiments, the centroid position of the diffraction-limited point spread function (PSF) for a fluorescent probe is determined using a maximum likelihood estimation method with a Gaussian mask estimated PSF (50). The distribution of centroid positions determined for the same probe over successive images (Fig. 2 *a*) is fit to a two-dimensional Gaussian (Fig. 2 *b*). Importantly, we observed a ~2× improvement in localization precision for Cy5-FDNs compared to single dyes, which is directly attributed to an increased number of photons collected from Cy5-FDNs (Fig. S1). For FDNs based on G5 PAMAM dendrimers conjugated with ~8 Cy5 dyes, we determined a localization precision of 6.0 nm (measured as s.d.), which corresponds to 14 nm in full width at half-maximum (FWHM) (Fig. 2, *a* and *b*). For FDNs based on G6 PAMAM dendrimers conjugated with ~14 Cy5 dyes, we determined the localization precision of 5.1 nm measured as the standard deviation (s.d.) over multiple localization events, which corresponds to 12 nm in FWHM. Using the same laser excitation and imaging conditions, we determined the localization precision for single Cy5 dyes to be 9.8 nm (measured as s.d.), which corresponds to 23 nm in FWHM (Fig. 2, *d* and *e*). Localization precision is often reported as the standard deviation of multiple localization events for a probe, whereas the spatial resolution is reported as the standard deviation (s.d.) or FWHM for multiple localizations (46,51). Overall, these experiments directly demonstrate that FDNs can be localized with superior precision compared to single organic dyes, which is extremely useful for high-resolution single-molecule localization or subcellular center-of-mass tracking experiments.

High-precision localization of fluorescent probes strongly depends on the total number of collected photons. Localization precision (δx) can be estimated by the expression: $\delta x^2 \approx (s^2 + c_1a^2)/N + c_2s^4b^2/a^2N^2$, where s is the standard deviation of the Gaussian fit to the PSF, N is the number of collected photons, b is standard deviation of the background, a is the pixel size of the detector and c_1 and c_2 are numerical constants (52). The statistics of Cy5-FDN probe brightness are shown in Fig. S1, which compares the total number of collected photons for single Cy5-FDNs and single Cy5 dyes. Together, these experiments show that Cy5-FDNs improve localization precision by significantly increasing the total number of photons (N) collected per probe compared to single organic dyes.

Bright fluorescent probes with improved photostability would greatly benefit fluorescence microscopy and

biological imaging. In a series of single-molecule experiments, we measured the photobleaching kinetics of FDNs compared to single organic dyes (Fig. 3 and Fig. S3). Photobleaching lifetimes are quantified by tracking individual fluorescence intensity traces from single FDNs and single dyes and recording the time required to bleach to a dark state under constant excitation. Fig. 3 *a* shows the active fraction of fluorescent molecules (Cy5-FDNs or Cy5 dyes) as a function of time, averaged over ~1000 molecule ensembles. The active, nonbleached fraction of Cy5-FDNs displayed a remarkably linear decay response, whereas the nonbleached fraction of single dyes fit to a single exponential decay, which is expected based on photobleaching statistics for single dyes (Fig. S4) (8). In this way, Cy5-FDNs remain bright and photoactive for extended durations, which can be useful to assay biological dynamics over longer periods of time in fluorescence microscopy experiments. We also observed extended photobleaching lifetimes for Cy3-FDNs (Fig. S3).

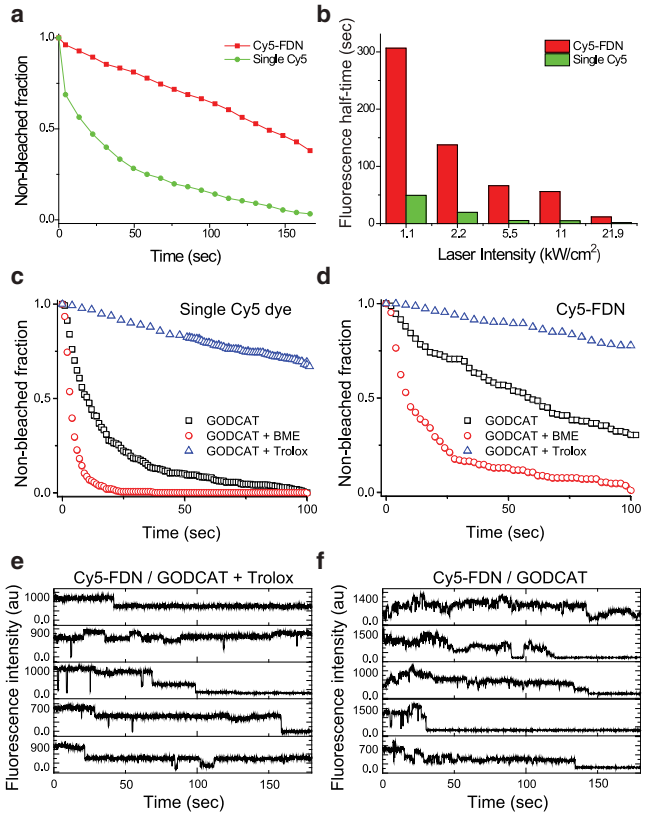

FIGURE 3 Single-molecule photobleaching kinetics for Cy5-FDNs and Cy5 molecules under the same excitation and imaging conditions. (*a*) Fraction of nonphotobleached fluorophores as a function of time for ~1000 molecule ensembles of Cy5-FDN and Cy5 molecules (2.2 kW/cm^2 intensity). (*b*) Fluorescence photobleaching lifetimes for single Cy5-FDNs and single Cy5 molecules as a function of laser excitation intensity. In (*a*) and (*b*), data was acquired in the presence of GODCAT as an oxygen scavenging system. (*c*) Single-molecule photobleaching kinetics for single Cy5 dyes in the presence of 1.0% (v/v) BME and 2 mM Trolox (6.6 kW/cm^2 intensity). (d) Single-molecule photobleaching kinetics for Cy5-FDNs in the presence of 1.0% (v/v) BME and 2 mM Trolox. (*e*) Single-molecule fluorescence emission traces (5 sample molecules) for Cy5-FDNs in the presence of Trolox. (*f*) Single-molecule fluorescence emission traces (5 sample molecules) for Cy5-FDNs in the absence of Trolox and BME.

Overall, FDNs exhibit significantly increased photobleaching lifetimes compared to single dye molecules. To evaluate the performance of Cy5-FDNs under different imaging conditions, we further characterized photobleaching lifetimes for Cy5-FDNs and single Cy5 dyes as a function of laser excitation intensity (Fig. 3 *b*). In these experiments, the fluorescence half-time is defined as the time required for 50% of the initial population to photobleach to an irreversible dark state. In all cases, the photobleaching lifetimes of single Cy5-FDNs far exceed the lifetimes of single Cy5 dyes. In particular, we observed a ~6–10× increase in photobleaching lifetimes for Cy5-FDNs based on G5 PAMAM dendrimers conjugated with ~8 Cy5 dyes. For laser excitation intensities typical for SMFM, approximately half of the Cy5-FDN population remains active after ~140 s of constant illumination (2.2 kW/cm^2), whereas half of the single Cy5 dye population photobleaches within ~15 s. Finally, we observed a ~17× increase in the photobleaching lifetimes for single Cy5-FDNs based on G6 PAMAM dendrimers conjugated with ~14 Cy5 dyes, compared to the photobleaching lifetime of single Cy5 dyes (Fig. S5). The photostability results shown in Fig. 3, *a* and *b*, and Fig. S5 were obtained for imaging in the presence of glucose oxidase/catalase (GODCAT), which is a coupled enzymatic system used to scavenge oxygen from solution. We also studied the fluorescence emission intensity of FDN probes in the presence of beta-mercaptoethanol (BME), a reducing agent known to suppress short timescale (millisecond) blinking events. The fraction of active Cy5 dyes and Cy5-FDNs in the presence of BME are shown in Fig. 3, *c* and *d*, respectively. Clearly, addition of BME substantially reduces the fraction of active or bright probes for both single Cy5 dyes and FDN probes, which is likely attributed to a decrease in probe brightness due to BME inducing long-lived dark states. We also observed the photobleaching behavior of Cy5-FDNs in the presence of Trolox, another reducing agent known to suppress the long-lived dark states (53). In the presence of Trolox, the photostability of Cy5-FDN probes is tremendously increased, as shown in Fig. 3 *d*. We further investigated the fluorescence emission intensity of single FDN probes in the presence (Fig. 3 *e*) and absence (Fig. 3 *f*) of Trolox, where five sample molecular traces for each condition are shown. Interestingly, single-molecule traces for Cy5-FDNs show that Trolox confers a marked increase in the stability of the fluorescence emission intensity for single FDN probes. In this way, FDN probes offer the dual advantage of increased brightness (due to multiple conjugated dyes) with increased photostability for single-molecule biophysics experiments when imaged in the presence of reducing agents such as Trolox, which will be

useful for single-molecule biophysics experiments based on fluorescence.

Although Cy5-FDNs are brighter than single organic dyes, the increase in probe brightness does not scale linearly with the average number of conjugated dyes per Cy5-FDN molecule. For example, Cy5-FDNs based on G5 PAMAM dendrimers show a ~2–5× increase in the number of collected photons relative to single Cy5 dyes, which does not match the average number Cy5 dyes per probe (~8) determined by MALDI-TOF MS (Table S1). To investigate fluorescence emission intensities for Cy5-FDNs, we measured the bulk fluorescence emission for Cy5-FDN samples and Cy5 dye samples at equivalent dye concentrations based on equal absorption (Fig. S6). Bulk fluorescence measurements showed that Cy5-FDN fluorescence emission was ~45% less intense (per dye molecule) compared to free Cy5 dye samples, which is in good agreement with single-molecule fluorescence data. If individual dye molecules on dendrimer scaffolds are independent, noninteracting fluorophores, then photobleaching lifetimes are not expected to increase compared to single dye molecules, and the fluorescence emission intensity of single Cy5-FDNs would scale linearly with the number of dye molecules conjugated to dendrimer surfaces. However, this is not the case for FDN dendrimer probes conjugated with multiple dyes. In addition, photophysical interactions between dyes on dendrimer scaffolds would complicate the determination of the distribution of dyes per dendrimer probe using single-molecule fluorescence emission data.

Collective photophysical effects would alter the emission properties of independent nearby dyes. Collective effects in multichromophoric systems such as natural light-harvesting complexes (54,55) or synthetic systems (28,56,57) can arise due to several photophysical mechanisms. Strong excitonic coupling can occur for dyes located in close proximity (<1 nm) (58), which results in splitting of the excited electronic state with new selection rules for electronic transitions, thereby yielding H-dimers with blue-shifted absorption and fluorescence quenching (59), or J-dimers with red-shifted absorption and enhanced fluorescence emission (58). Weak excitonic coupling can occur for larger interchromophoric spacings (~1–2 nm), resulting in reduced fluorescence emission but no observable change in absorption spectra (56). For Cy5-FDNs based on G5 dendrimers conjugated with 8 dyes, the maximum interchromophoric spacing between two individual dyes on a single Cy5-FDN is ~3–4 nm (based on geometrical considerations), which allows for the possibility of strong or weak excitonic coupling. However, strong excitonic coupling is unlikely, because the bulk absorption spectrum for FDN samples is neither blue- nor red-shifted compared to free Cy5 dye (Fig. S7) or to FDNs labeled with only ~1 Cy5 dye per probe (Fig. S8). On the other hand, weak excitonic coupling is supported by single-molecule experiments. Single-molecule fluorescence intensity traces show that a subpopulation of Cy5-FDNs exhibits structured, stepwise photobleaching behavior, whereas a separate subpopulation shows broad, unstructured fluorescence intensities. Unstructured fluorescence intensity traces have been attributed to weak excitonic coupling interactions for aromatic dendrimers labeled with multiple dyes (28,57), which may explain the reduced fluorescence emission observed for Cy5-FDNs (Fig. S6). Moreover, weak coupling interactions could also explain the nonexponential photobleaching behavior for Cy5-FDNs shown in Fig. 3 *a*. To explore this phenomenon further, we synthesized Cy5-FDNs containing an average of ~1 Cy5 dye on G5 PAMAM scaffolds. We observed that the photobleaching half-time for Cy5-FDNs containing ~1 Cy5 dye was similar to the photobleaching half-time of single (free) Cy5 dyes, which suggests that putative interactions between Cy5 molecules and dendritic scaffolds do not give rise to altered photophysical effects such as enhanced photostability (Fig. S8). Based on these results, we attribute the extended photobleaching lifetimes to weak coupling interactions between dye molecules on dendritic nanoprobes.

Beyond photophysical characterization, we demonstrated proof-of-principle application of Cy5-FDNs to single-molecule fluorescence imaging. In particular, we used Cy5-FDNs as fluorescent probes in a SiMPull assay, which allows for target-specific capture and quantification of proteins at the single-molecule level (Fig. 4) (38). Single-molecule images were obtained using TIRF-M, as shown in the schematic of the experimental setup in Fig. 4 *a*. First, mouse and bovine secondary antibodies were conjugated with Cy5-FDNs using copper-free click chemistry (see the Supporting Material). Next, antibiotin primary antibody (mouse) was immobilized on biotin-serum-coated glass coverslip surfaces, followed by incubation of Cy5-FDN-secondary antibody (mouse or bovine) to allow for target-specific protein capture. The average number of target mouse Cy5-FDN-secondary antibodies in a field of view was 320 ± 36 (mouse primary antibody), which far exceeds the number of surface-bound molecules in control experiments (bovine primary antibody, 7 ± 7; no mouse primary antibody, 22 ± 9; no bovine primary antibody, 7 ± 4) (Fig. 4 *b*). Fig. 4 *c* shows representative images from the single-molecule pull-down assay, which clearly show highly specific protein capture as revealed by Cy5-FDN probes. In the single-molecular pull-down assay, we also used two-color fluorescence colocalization between Cy3-primary antibodies and Cy5-FDN-secondary antibodies to directly demonstrate high fidelity protein capture between target proteins (Fig. 4 *d*).

In addition to single-molecule protein capture experiments, we also used FDN probes for conventional immunofluorescence imaging, which further demonstrates proof-of-principle application of FDN probes to biological imaging (Fig. 5). In this experiment, we imaged the microtubule cytoskeleton in mammalian cells (HEK293) by

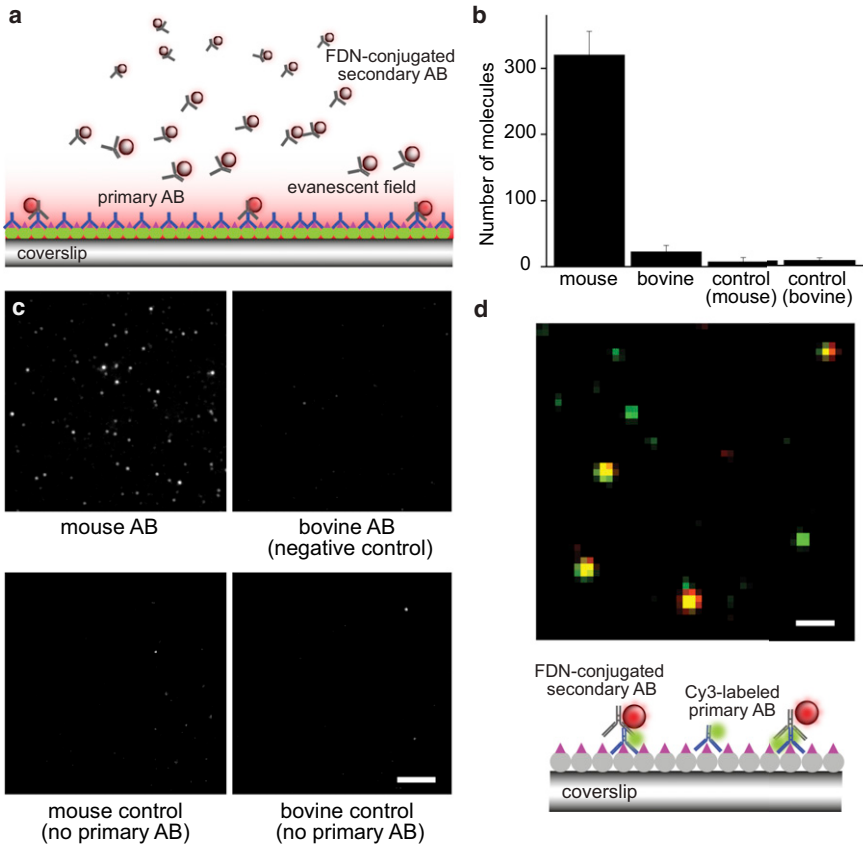

FIGURE 4 SiMPull assay using Cy5-FDNs as fluorescent probes. (*a*) Schematic of single-molecule experimental scheme. Antibiotin primary AB was incubated with surfaces treated with biotinylated serum, followed by incubation of Cy5-FDN-conjugated secondary AB targeting mouse IgG and bovine IgG. (*b*) The SiMPull assay was quantified by counting the average numbers of bound ABs per field of view for target (mouse secondary) and negative control experiments. (*c*) Single-molecule images of the SiMPull assay, which clearly show high degrees of specific protein capture and low amounts of nonspecific interactions. Images were acquired using TIRF-M. Scale bar: 6 μm. (*d*) Single-molecule fluorescence colocalization experiments showing spatial colocalization between Cy3-labeled primary antibodies and Cy5-FDN-labeled mouse secondary antibodies. In these experiments, Cy3-primary antibodies and Cy5-FDN secondary antibodies were mixed in a 1:1 molar ratio and immobilized on the biotin-serum bound surface. For display, Cy3 molecules and Cy5-FDNs are pseudocolored as green and red, respectively. Scale bar: 1 μm.

immunofluorescence microscopy using Cy5-FDN-conjugated antibodies. Microtubule networks in fixed HEK293 cells were labeled using a primary anti-alpha-tubulin antibody (clone AA13, mouse), followed by incubation with Cy5-FDN-conjugated secondary antibodies (antimouse). To facilitate labeling, secondary antibodies were modified with azide moieties via azide-NHS ester linkers, followed by direct conjugation to Cy5-FDNs by copper-free click chemistry. For labeling studies, we adjusted the Cy5-FDN-to-antibody stoichiometry to 0.4:1 (FDN:protein) to avoid conjugation of multiple Cy5-FDNs to secondary antibodies, whereas single Cy5 dyes were conjugated to secondary antibodies using a 0.9:1 (dye:protein) stoichiometry. Fig. 5 shows immunofluorescence images of microtubule networks obtained using both Cy5-FDN-conjugated and Cy5-conjugated secondary antibodies. Immunofluorescence images show that conventional, single organic dye-conjugated antibodies photobleach rapidly when obtained using moderate to high excitation intensity. However, immunofluorescence images obtained using Cy5-FDN-conjugated secondary antibodies showed vastly improved photostability, which agrees with photophysical characterization of Cy5-FDNs (Fig. 3). Fluorescence images shown in Fig. 5 were acquired using relatively high excitation intensity (22 kW/cm^2), such that single Cy5 dyes photobleached after only a few seconds of constant exposure, whereas Cy5-FDNs remained fluorescent in excess of 120 s of exposure under the same illumination conditions. In general, secondary antibodies have a limited number of lysine or cysteine reactive sites to facilitate fluorescent probe conjugation, and labeling antibodies with FDNs uses fewer reactive sites given the same brightness increase relative to single organic dyes. Therefore, our results suggest that the quality of immunofluorescence images can be enhanced and acquired over longer periods of time using antibodies conjugated with FDNs.

Based on our experiments, FDN probes provide several advantages over labeling antibodies with single organic dyes for SiMPull protein capture experiments or conventional immunofluorescence imaging. In our experiments using FDN probes, we found that labeling secondary antibodies with dendritic nanoprobes neither hinders functionality nor significantly reduces specificity, which suggests that Cy5-FDNs can be used for target-specific protein labeling. In this way, FDN probes offer the dual advantage of increased probe brightness with minimal protein modification, which is useful in retaining functionality for antibody binding and protein capture experiments. For example, in conducting SiMPull experiments, antibodies generally need to be heavily labeled with multiple dye molecules to achieve increased fluorescence emission using organic dyes. However, extensive modifications to secondary antibodies are known to reduce binding affinity and disrupt antigenicity and function. By conjugating only

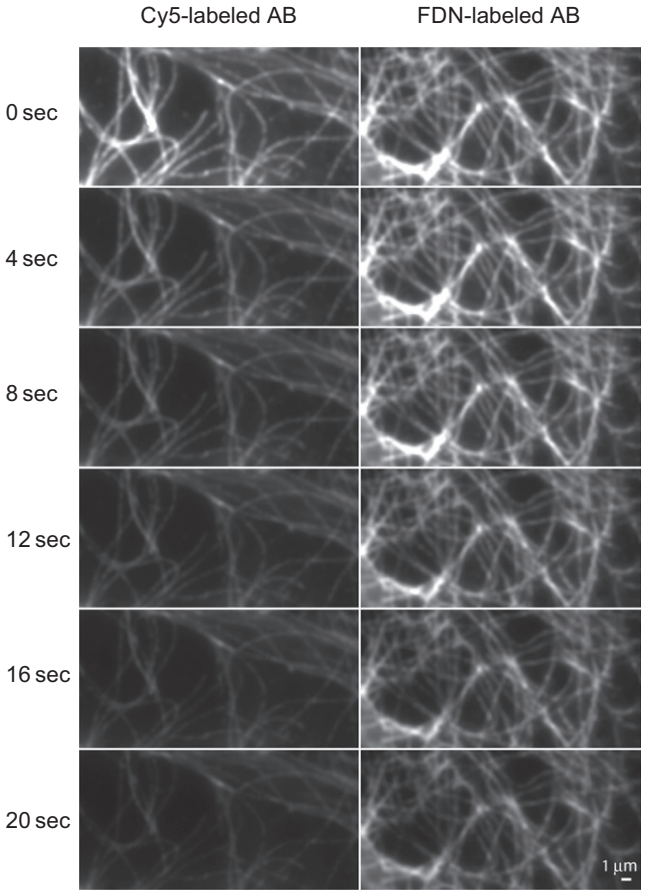

FIGURE 5 Immunofluorescence imaging of cytoskeletal networks in mammalian cells using Cy5-FDN-conjugated antibodies. Microtubules were immunostained with Cy5-FDN or Cy5-conjugated secondary antibodies. Time-lapse fluorescence microscopy images of immunolabeled microtubules show a marked increase in photostability for Cy5-FDN-conjugated antibodies compared to Cy5-labeled antibodies. Images were obtained using the same excitation and imaging conditions (22 kW/cm^2, in the presence of the GODCAT oxygen scavenger system). The concentration of secondary antibody was maintained constant in both experiments, and the labeling ratio was 0.4:1 and 0.9:1 probe:antibody for Cy5-FDN and Cy5 probes, respectively.

a single FDN probe to a single antibody, we achieve brighter fluorescence emission and increased signal/noise per antibody. Finally, in our experiments, we observed no significant nonspecific interactions between FDN probes and proteins during binding, capture, or immunofluorescence imaging experiments.

In a final set of experiments, we used Cy5-FDNs as probes to assay single-molecule nucleic acid hybridization (Fig. 6). In this experiment, we performed two-color fluorescence imaging experiments to study the hybridization between two complementary DNA oligonucleotides. Here, a surface-bound oligo labeled with a Cy3 dye was hybridized to the complementary DNA oligo labeled with a Cy5-FDN probe (Fig. 6, *a* and *b*). First, single-stranded DNA oligonucleotides containing a Cy3 dye and biotin at the 5′ and 3′ termini, respectively, were specifically linked

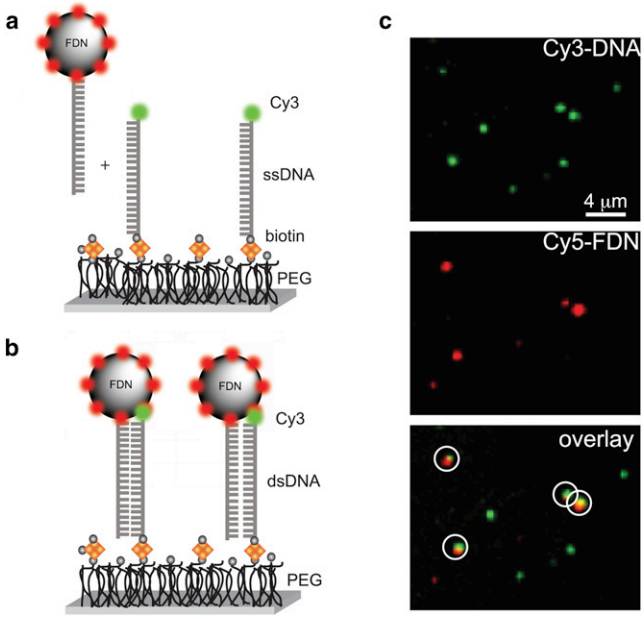

FIGURE 6 Single-molecule DNA hybridization assay using Cy5-FDNs as fluorescent probes. (*a*) Schematic of the single-molecule experimental setup. Cy3-labeled DNA was immobilized on PEGylated surfaces using biotin-NeutrAvidin linkages. (*b*) Cy5-FDN labeled DNA complementary to the surface bound oligos was introduced to allow for DNA hybridization. (c) Single-molecule images obtained during the DNA hybridization assay, which show DNA hybridization as evidenced by Cy3/Cy5-FDN colocalization.

to NeutrAvidin-treated PEG/PEG biotin coverslips. Individual Cy3-labeled DNA molecules on the surface were imaged and localized using TIRF-M. Next, a single-stranded DNA oligo complementary to the surface-bound strand containing a Cy5-FDN at the 3′ terminus was incubated for 5 min to allow for DNA hybridization. The DNA hybridization reaction was performed in a binding buffer containing bovine serum albumin and nonspecific nucleic acids, which minimizes nonspecific binding of the target oligo. Finally, the coverslip surfaces were rinsed copiously with buffer, and single-molecule images were obtained.

In this experiment, DNA hybridization events are visualized at the single-molecule level by colocalization of green (Cy3 channel) and red (Cy5-channel) emission. Fig. 6 *c* shows that single-molecule images of Cy3-DNA and FDN-Cy5-DNA overlap, which suggests that the complementary strands of DNA are efficiently hybridized. Our results show that the emission of FDN-Cy5 co-localizes with Cy3 dye with high frequency during DNA hybridization experiments and not during control experiments using only FDN probes and Cy3 dyes. High fidelity of colocalization precludes nonspecific interactions as the dominant mechanism for DNA binding. Taken together with the enhanced photobleaching times for FDN probes compared to single dyes (Fig. 3), these results suggest that FDNs can be an attractive option for single-molecule

nucleic acid labeling and DNA localization experiments due to the extended data acquisition period compared to single organic dyes.

In this work, we present dendritic nanoconjugates as molecular-scale fluorescent probes for SMFM. We characterized the photophysical properties of FDNs, and we demonstrate the direct application of these probes to DNA and protein assays. Dendrimers function as molecular scaffolds to effectively package multiple dye molecules into single, nanometer-sized macromolecules. Single-molecule fluorescence measurements reveal that FDNs exhibit enhanced photostability, brightness, and localization precision compared to single organic dye molecules. It is important to note that these advantageous photophysical properties are achieved using small nanoscale probes (~5 nm), significantly smaller in size compared to large fluorescent beads (~40–1000+ nm) or biocompatible semiconductor nanocrystals (~20 nm). There is a strong need for development of advanced fluorescent probes with small nanoscale dimensions for biological imaging. Of course, fluorescent beads can be localized with precisions below the diffraction limit, albeit at the cost of conjugating extremely large probes to small biomolecules such as DNA, RNA, or proteins (~1–5 nm). Bulky probes do not reveal the true locations of the biomolecules, and large probes may interfere with biological function. Single organic dyes are small molecule probes (<1 nm), however, it can be challenging to achieve nanometer-scale localization precision (1–10 nm) using organic dyes due to the limited number of photons collected per imaging event or before dyes bleach to an irreversible dark state. From this perspective, FDNs offer the combined advantages of enhanced photophysical properties and small nanoscale dimensions, which can benefit a wide array of advanced high-resolution imaging techniques and subdiffraction localization methods (48,51). Given the relatively small size and improved brightness of FDNs, these probes feature potential benefits for both single-molecule experiments and general fluorescence imaging (5,45,46), including extended observation periods during sample imaging. Based on our results and proof-of-principle application of FDNs to biological imaging, dendritic nanoprobes appear to hold strong potential to serve as a new, to our knowledge, class of fluorescent probes for biological assays and imaging.

SUPPORTING MATERIAL

Supporting materials and methods, figures and analysis are available at http://www.biophysj.org/biophysj/supplemental/S0006-3495(13)00185-9.

We thank Nam-Ho Kim for simulations, Nicolette Iatropoulos for data analysis, and Sam Lord for useful discussions.

This work was supported by a Packard Fellowship from the David and Lucile Packard Foundation (to C.M.S.), a National Institutes of Health (NIH) Pathway to Independence Award (4R00HG004183-03 to C.M.S.), and an NIH MERIT Award (5R37DK015556 to J.A.K.).

REFERENCES

1. Selvin, P. R., and T. Ha. 2008. Single-Molecule Techniques: A Laboratory Manual. Cold Spring Harbor Laboratory Press, New York.
2. Betzig, E., G. H. Patterson, …, H. F. Hess. 2006. Imaging intracellular fluorescent proteins at nanometer resolution. *Science.* 313:1642–1645.
3. Hell, S. W. 2007. Far-field optical nanoscopy. *Science.* 316:1153–1158.
4. Xie, X. S., P. J. Choi, …, G. Lia. 2008. Single-molecule approach to molecular biology in living bacterial cells. *Annu. Rev. Biophys.* 37:417–444.
5. Huang, B., H. Babcock, and X. Zhuang. 2010. Breaking the diffraction barrier: super-resolution imaging of cells. *Cell.* 143:1047–1058.
6. Lord, S. J., H. L. Lee, and W. E. Moerner. 2010. Single-molecule spectroscopy and imaging of biomolecules in living cells. *Anal. Chem.* 82:2192–2203.
7. Shaner, N. C., R. E. Campbell, …, R. Y. Tsien. 2004. Improved monomeric red, orange and yellow fluorescent proteins derived from *Discosoma* sp. red fluorescent protein. *Nat. Biotechnol.* 22:1567–1572.
8. Roy, R., S. Hohng, and T. Ha. 2008. A practical guide to single-molecule FRET. *Nat. Methods.* 5:507–516.
9. Bruchez, Jr., M., M. Moronne, …, A. P. Alivisatos. 1998. Semiconductor nanocrystals as fluorescent biological labels. *Science.* 281:2013–2016.
10. Chan, W. C. W., and S. Nie. 1998. Quantum dot bioconjugates for ultrasensitive nonisotopic detection. *Science.* 281:2016–2018.
11. Benesch, R. E., and R. Benesch. 1953. Enzymatic removal of oxygen for polarography and related methods. *Science.* 118:447–448.
12. Rasnik, I., S. A. McKinney, and T. Ha. 2006. Nonblinking and long-lasting single-molecule fluorescence imaging. *Nat. Methods.* 3:891–893.
13. Vogelsang, J., R. Kasper, …, P. Tinnefeld. 2008. A reducing and oxidizing system minimizes photobleaching and blinking of fluorescent dyes. *Angew. Chem. Int. Ed. Engl.* 47:5465–5469.
14. Ekimov, A., and A. Onushchenko. 1981. Quantum size effect in three-dimensional microscopic semiconductor crystals. *JETP Lett.* 34:345–349.
15. Michalet, X., F. F. Pinaud, …, S. Weiss. 2005. Quantum dots for live cells, in vivo imaging, and diagnostics. *Science.* 307:538–544.
16. Nirmal, M., B. Dabbousi, …, L. Brus. 1996. Fluorescence intermittency in single cadmium selenide nanocrystals. *Nature.* 383:802–804.
17. Wang, X., X. Ren, …, T. D. Krauss. 2009. Non-blinking semiconductor nanocrystals. *Nature.* 459:686–689.
18. Wang, F., W. B. Tan, …, M. Wang. 2006. Luminescent nanomaterials for biological labelling. *Nanotechnology.* 17:R1–R13.
19. Majoros, I. J., A. Myc, …, J. R. Baker, Jr. 2006. PAMAM dendrimer-based multifunctional conjugate for cancer therapy: synthesis, characterization, and functionality. *Biomacromolecules.* 7:572–579.
20. Frechet, J. M. J., D. A. Tomalia, …, I. Sons. 2001. Dendrimers and Other Dendritic Polymers. Wiley, New York.
21. Koo, O. M., I. Rubinstein, and H. Onyuksel. 2005. Role of nanotechnology in targeted drug delivery and imaging: a concise review. *Nanomedicine.* 1:193–212.
22. Talanov, V. S., C. A. S. Regino, …, M. W. Brechbiel. 2006. Dendrimer-based nanoprobe for dual modality magnetic resonance and fluorescence imaging. *Nano Lett.* 6:1459–1463.
23. Balzani, V., S. Campagna, …, M. Venturi. 1998. Designing dendrimers based on transition-metal complexes. Light-harvesting properties and predetermined redox patterns. *Acc. Chem. Res.* 31:26–34.
24. Adronov, A., S. L. Gilat, …, G. R. Fleming. 2000. Light harvesting and energy transfer in laser-dye-labeled poly (aryl ether) dendrimers. *J. Am. Chem. Soc.* 122:1175–1185.
25. Adronov, A., and J. M. J. Frechet. 2000. Light-harvesting dendrimers. *Chem. Commun.* 1701–1710.

26. Watson, M. D., A. Fechtenkötter, and K. Müllen. 2001. Big is beautiful—"aromaticity" revisited from the viewpoint of macromolecular and supramolecular benzene chemistry. *Chem. Rev.* 101:1267–1300.
27. Swallen, S., R. Kopelman, …, C. Devadoss. 1999. Dendrimer photoantenna supermolecules: energetic funnels, exciton hopping and correlated excimer formation. *J. Mol. Struct.* 485:585–597.
28. Hofkens, J., M. Maus, …, F. De Schryver. 2000. Probing photophysical processes in individual multichromophoric dendrimers by single-molecule spectroscopy. *J. Am. Chem. Soc.* 122:9278–9288.
29. Minard-Basquin, C., T. Weil, …, K. Müllen. 2003. A polyphenylene dendrimer-detergent complex as a highly fluorescent probe for bioassays. *J. Am. Chem. Soc.* 125:5832–5838.
30. Oesterling, I., and K. Müllen. 2007. Multichromophoric polyphenylene dendrimers: toward brilliant light emitters with an increased number of fluorophores. *J. Am. Chem. Soc.* 129:4595–4605.
31. Boas, U., and P. M. H. Heegaard. 2004. Dendrimers in drug research. *Chem. Soc. Rev.* 33:43–63.
32. Svenson, S., and D. A. Tomalia. 2005. Dendrimers in biomedical applications—reflections on the field. *Adv. Drug Deliv. Rev.* 57:2106–2129.
33. Liu, H., T. Toring, …, K. V. Gothelf. 2010. DNA-templated covalent coupling of G4 PAMAM dendrimers. *J. Am. Chem. Soc.* 132:18054–18056.
34. Weil, T., U. M. Wiesler, …, K. Müllen. 2001. Polyphenylene dendrimers with different fluorescent chromophores asymmetrically distributed at the periphery. *J. Am. Chem. Soc.* 123:8101–8108.
35. Balogh, L., and D. A. Tomalia. 1998. Poly (amidoamine) dendrimer-templated nanocomposites. 1. Synthesis of zerovalent copper nanoclusters. *J. Am. Chem. Soc.* 120:7355–7356.
36. Caminade, A. M., A. Hameau, and J. P. Majoral. 2009. Multicharged and/or water-soluble fluorescent dendrimers: properties and uses. *Chemistry.* 15:9270–9285.
37. Jewett, J. C., and C. R. Bertozzi. 2010. Cu-free click cycloaddition reactions in chemical biology. *Chem. Soc. Rev.* 39:1272–1279.
38. Jain, A., R. Liu, …, T. Ha. 2011. Probing cellular protein complexes using single-molecule pull-down. *Nature.* 473:484–488.
39. Yildiz, A., J. N. Forkey, …, P. R. Selvin. 2003. Myosin V walks hand-over-hand: single fluorophore imaging with 1.5-nm localization. *Science.* 300:2061–2065.
40. Estrada, L. C., and E. Gratton. 2011. 3D nanometer images of biological fibers by directed motion of gold nanoparticles. *Nano Lett.* 11:4656–4660.
41. Kural, C., H. Kim, …, P. R. Selvin. 2005. Kinesin and dynein move a peroxisome in vivo: a tug-of-war or coordinated movement? *Science.* 308:1469–1472.
42. Rittweger, E., K. Y. Han, …, S. W. Hell. 2009. STED microscopy reveals crystal colour centres with nanometric resolution. *Nat. Photonics.* 3:144–147.
43. Hell, S. W., and J. Wichmann. 1994. Breaking the diffraction resolution limit by stimulated emission: stimulated-emission-depletion fluorescence microscopy. *Opt. Lett.* 19:780–782.
44. Gustafsson, M. G. L. 2005. Nonlinear structured-illumination microscopy: wide-field fluorescence imaging with theoretically unlimited resolution. *Proc. Natl. Acad. Sci. USA.* 102:13081–13086.
45. Huang, B., W. Wang, …, X. Zhuang. 2008. Three-dimensional super-resolution imaging by stochastic optical reconstruction microscopy. *Science.* 319:810–813.
46. Rust, M. J., M. Bates, and X. Zhuang. 2006. Sub-diffraction-limit imaging by stochastic optical reconstruction microscopy (STORM). *Nat. Methods.* 3:793–795.
47. Fölling, J., M. Bossi, …, S. W. Hell. 2008. Fluorescence nanoscopy by ground-state depletion and single-molecule return. *Nat. Methods.* 5:943–945.
48. Manley, S., J. M. Gillette, …, J. Lippincott-Schwartz. 2008. High-density mapping of single-molecule trajectories with photoactivated localization microscopy. *Nat. Methods.* 5:155–157.
49. Patterson, G. H., and J. Lippincott-Schwartz. 2002. A photoactivatable GFP for selective photolabeling of proteins and cells. *Science.* 297:1873–1877.
50. Mortensen, K. I., L. S. Churchman, …, H. Flyvbjerg. 2010. Optimized localization analysis for single-molecule tracking and super-resolution microscopy. *Nat. Methods.* 7:377–381.
51. Jones, S. A., S. H. Shim, …, X. Zhuang. 2011. Fast, three-dimensional super-resolution imaging of live cells. *Nat. Methods.* 8:499–508.
52. Thompson, R. E., D. R. Larson, and W. W. Webb. 2002. Precise nanometer localization analysis for individual fluorescent probes. *Biophys. J.* 82:2775–2783.
53. Ha, T., and P. Tinnefeld. 2012. Photophysics of fluorescent probes for single-molecule biophysics and super-resolution imaging. *Annu. Rev. Phys. Chem.* 63:595–617.
54. Goldsmith, R. H., and W. E. Moerner. 2010. Watching conformational- and photo-dynamics of single fluorescent proteins in solution. *Nat. Chem.* 2:179–186.
55. van Oijen, A. M., M. Ketelaars, …, J. Schmidt. 1999. Unraveling the electronic structure of individual photosynthetic pigment-protein complexes. *Science.* 285:400–402.
56. Hernando, J., M. van der Schaaf, …, N. F. van Hulst. 2003. Excitonic behavior of rhodamine dimers: a single-molecule study. *J. Phys. Chem. A.* 107:43–52.
57. Vosch, T., J. Hofkens, …, F. C. De Schryver. 2001. Influence of structural and rotational isomerism on the triplet blinking of individual dendrimer molecules. *Angew. Chem.* 113:4779–4784.
58. Kasha, M., H. Rawls, and M. A. El-Bayoumi. 1965. The exciton model in molecular spectroscopy. *Pure Appl. Chem.* 11:371–392.
59. Conley, N. R., A. K. Pomerantz, …, W. E. Moerner. 2007. Bulk and single-molecule characterization of an improved molecular beacon utilizing H-dimer excitonic behavior. *J. Phys. Chem. B.* 111:7929–7931.